Materials Advances

ROYAL SOCIETY OF CHEMISTRY

PAPER

View Article Online
View Journal | View Issue

Cite this: *Mater. Adv.*, 2025, **6**, 8139

Enhanced adsorption of an organic dye by phyto-synthesized CuO nanoparticles derived from *Malva sylvestris* for sustainable environmental remediation

Ahmad Jaddo Mohammed Ameen, [ad] Khalid M. Omer [*bc] and Amin K. Qasim[d]

This study presents the green synthesis of copper oxide (CuO) nanoparticles using *Malva sylvestris* extract as a biogenic reducing and stabilizing agent, offering an eco-friendly and sustainable route to nanoparticle production. The synthesized CuO nanoparticles were thoroughly characterized through advanced analytical techniques to elucidate their morphology, crystalline structure, and surface properties. These nanoparticles were subsequently employed as an efficient adsorbent for the removal of Congo red dye from aqueous solutions. The adsorption process was systematically optimized by investigating the effects of pH, contact time, adsorbent dosage, and initial dye concentration. Kinetic studies indicated that the adsorption followed a pseudo-second-order model (R^2 = 0.9997), suggesting that chemisorption was the predominant mechanism. Equilibrium data showed excellent correlation with both Langmuir and Freundlich isotherm models (R^2 > 0.99), implying the coexistence of monolayer and multilayer adsorption processes. Thermodynamic parameters revealed that the adsorption was spontaneous and exothermic (ΔH° = −34.35 kJ mol^{-1}), accompanied by reduction in entropy (ΔS° = −106.46 J mol^{-1} K^{-1}), supporting a combination of physical and chemical adsorption mechanisms. The CuO nanoparticles demonstrated a maximum adsorption capacity of 6.99 mg g^{-1} for Congo red under optimized conditions: 4 ppm dye concentration, pH 7.0, temperature 20 °C, and 0.02 g adsorbent per 10 mL solution, achieving equilibrium within 30 minutes. The CuO nanoparticles retained over 78% of their adsorption efficiency after four regeneration cycles, highlighting their reusability and potential for long-term applications. Overall, the findings underscore the significant adsorption capability and environmental compatibility of phyto-synthesized CuO nanoparticles, positioning them as a promising candidate for sustainable wastewater treatment technologies.

Received 1st July 2025,
Accepted 24th September 2025

DOI: 10.1039/d5ma00697j

rsc.li/materials-advances

1. Introduction

Nanoparticles with grain sizes less than 100 nm are now attracting a lot of attention in a number of different sectors. This is because of the significance of their physico-chemical characteristics in comparison to the bulk materials. These characteristics include, for instance, tunable bandgap energies, which enhance optical and electronic properties, zeta potential, which governs colloidal stability, and interfacial interactions, factors that are critical in applications such as adsorption, catalysis, and biomedicine.[1] Nanoparticles possess several applications; this is attributed to their unique features; they also vary in size, shape, and dimensions, as well as in their composition.[2]

Many nanomaterials, such as nanocomposites, carbon-based nanomaterials, and metal–organic frameworks (MOFs), have been prepared for various applications in fields such as energy, sensing, environment, and biomedicine.[3–7] Many metallic elements have a tendency to react with oxygen under a wide range of circumstances, resulting in the formation of metal oxides with various structural configurations. Metal oxide nanoparticles (MONPs) are nanoscale particles consisting of metal atoms linked to oxygen atoms, exhibiting extraordinary properties owing to their unique compositional structure. The structure of MONPs can vary, predominantly exhibiting crystal structures such as cubic or tetragonal shaped structures.

[a] *Department of Biology, College of Education, Akre University for Applied Science, Kurdistan Region, Iraq*
[b] *Department of Chemistry, College of Science, University of Sulaimani, Qlisan Street, Sulaymaniyah, 46002, Kurdistan region, Iraq. E-mail: Khalid.omer@univsul.edu.iq*
[c] *Basic Sciences Research Center (BSRC), Deanship of Scientific Research, Imam Mohammad Ibn Saud Islamic University (IMSIU), P.O. Box 90950, Riyadh, 11623, Saudi Arabia*
[d] *Department of Chemistry, Faculty of Science, University of Zakho, Kurdistan Region, Iraq*

MONPs can crystallize in various polymorphic forms, with cubic and monoclinic structures being among the most common. These structural variations strongly influence their surface properties and functional behavior. Cubic oxides generally exhibit high symmetry and dense packing, which contributes to better thermal stability but may limit the availability of active surface sites for adsorption or catalysis. On the other hand, monoclinic oxides possess lower symmetry and more distorted coordination environments, often resulting in enhanced surface reactivity, greater defect density, and improved adsorption capacity. These differences in crystal geometry directly impact their performance in applications such as environmental remediation and heterogeneous catalysis.[8,9]

Their morphology plays a vital role in influencing functioning and reactivity for diverse applications.[10,11] The effects of these nanostructures on medicine, chemistry, physics, information technology, energy storage, catalysis, sensing, and materials science have prompted research into their synthesis. MONPs and similar nanocomposites have been studied extensively for their characteristics and applications; characteristics such as controllable morphologies, distinctive crystalline nature, flexible surface chemistry, high stability, specific catalytic activity, and customizable band edges make MONPs effective instruments for many different applications.[11–14]

Nowadays, transition metal oxide nanoparticles are the most commonly utilized nanoparticles; for instance, the oxides of iron, nickel, zinc, and copper occupy an extremely important place in different fields.[15–18] Cupric oxide (CuO), among transition metal oxides, is noteworthy for its distinctive properties and has been utilized in various applications, including gas sensors,[19] biosensors,[20] catalysis,[21] wastewater treatment, batteries and energetic materials.[22] The extensive use of this material stems from its notable attributes, including stability, cost-effectiveness, plenteousness, hydrophilicity, nontoxicity, and the straightforward synthesis of diverse nanoparticles in varied sizes and forms (*e.g.*, floral, spherical, and nanorods).[23,24]

The three primary prerequisites for nanoparticle production are the selection of a green or environmentally friendly solvent (*e.g.*, water or ethanol), a non-toxic stabilizing substance (such as plant polysaccharides or starch), and an efficient reducing agent (commonly found in plant extracts, like flavonoids, polyphenols, or ascorbic acid).[25]

Various synthetic methods, including chemical methods, physical methods, and biosynthetic approaches, have been widely used for nanoparticle creation. Chemical and physical synthesis methods are often unsafe, technically demanding, hard, and expensive and involve the use of dangerous and harmful chemicals, which cause significant environmental risks.[26,27] The green synthesis pathway is a safe, biocompatible, and environmentally sustainable method for synthesizing nanoparticles utilizing plants and microbes for many applications.[28,29] The biosynthesis can be carried out using bacteria,[30] algae,[31] fungi[32] and plants. Different plant parts such as seeds, roots, stems, fruits, and leaves have been extensively employed for the synthesis of diverse nanomaterials. This is largely attributed to the presence of abundant phytochemicals in plant extracts, which serve as both reducing and stabilizing agents during nanoparticle formation.[33,34]

Plant-derived phytochemicals play a crucial and elegant role in the green synthesis of nanoparticles. Compounds such as flavonoids, phenolic acids, tannins, and terpenoids naturally present in leaves and other plant parts help reduce metal ions by acting as electron donors. At the same time, these molecules gently wrap around the newly formed nanoparticles, stabilizing them and preventing unwanted clumping. This dual function, reduction and stabilization, makes plant extracts powerful tools for producing nanoparticles in a simple, eco-friendly, and efficient manner.[35,36] Therefore, it is of great importance to use a green, low-cost route for production of the desired nanoparticle.

Freshwater is a vital component for human existence. Nonetheless, the sources of clean water are contaminated because of increasing worldwide population, urbanization, and industrialization, accompanied by many forms of domestic and industrial wastes.[37] Recently, wastewater polluted with artificial dyes has attracted considerable global interest due to the persistence and limited biodegradability of these dyes, posing possible environmental and health risks arising from their carcinogenic, mutagenic, and toxic properties.[38] Moreover, these dyes obstruct the penetration of sunlight, adversely affecting the process of photosynthesis and development of plants, elevating chemical and biological oxygen requirement and thus degrading the aesthetic qualities of aquatic ecosystems.[39] Adding to that, these dyes may aggravate respiratory conditions and induce skin irritation.[40] The enduring existence of these dyes in the environment demands the development of novel treatment strategies for their removal from aquatic systems.[41] Thus, the pressing need for creative, environmentally sustainable, economical, and enduring wastewater treatment solutions has become vital for guaranteeing the sustained supply of fresh water.

Among different methods for dye treatment, the techniques based on adsorption are extensively recognized.[42] Lately, researchers working on wastewater treatment have redirected their attention towards adsorbent materials that prioritize sustainability, quick adsorption rates, economic viability, and superior adsorptive efficacy.[43] A number of significant materials, including MONPs, carbon nanomaterials, activated carbon,[44] natural minerals,[45] and MOFs,[46,47] have been widely investigated for dye remediation in contaminated water.

Congo red (CR) is a synthetic azo dye widely used in the textile and printing industries. It is environmentally persistent and resistant to biodegradation, leading to long-term contamination of water bodies. Beyond its ecological impact, CR poses serious health risks due to its potential mutagenic and carcinogenic effects. Its metabolic byproducts, including benzidine, are known to be toxic and have been linked to cancer in humans. For these reasons, CR is classified as a hazardous substance by environmental authorities, and its removal from wastewater is considered a priority for environmental remediation.[48,49]

M. sylvestris has been selected in this research for its bioactive chemicals, which reduce and stabilize nanoparticles in green manufacturing. Accessibility, biocompatibility,

and therapeutic qualities enable its usage in sustainable nanotechnology.[50]

Despite various studies on CuO nanoparticles for dye removal, limited research has focused on using *Malva sylvestris* leaf extract as a green, bioactive precursor for nanoparticle synthesis. This plant offers unique phytochemicals that may enhance particle morphology and adsorption performance.[51] Moreover, our integrated evaluation of adsorption behavior with kinetic, isotherm, and thermodynamic modeling, coupled with regeneration analysis, distinguishes this work as a comprehensive and eco-conscious approach to dye remediation.

Recent studies have explored functionalized nanomaterials for dye removal. For instance, Debnath and Sinha developed polymer-based ZnO and hematite–PANI nanocomposites for dye removal, employing ultrasound-assisted synthesis and emphasizing adsorption kinetics and cost evaluation.[52,53] In contrast, our study presents the green synthesis of CuO nanoparticles using *Malva sylvestris* extract, offering a unique phytochemical approach. Furthermore, we combine adsorption modeling with thermodynamic analysis and regeneration assessment, providing a more environmentally sustainable and functionally comprehensive strategy for dye remediation.

Hence, the aim of our research is to synthesize CuO nanoparticles using an effective green synthesis method involving the *M. sylvestris* leaf extract. The synthesized CuO nanoparticles are evaluated as an adsorptive nanomaterial for removing CR dye from water, alongside modeling experimental outcomes using isotherm and kinetic models and thermodynamic studies. The nanoparticle is finally regenerated and reused against the CR dye to show its stability and efficiency.

2. Experimental part

2.1. Materials

All chemicals employed were of analytical grade and used without further purification. Copper nitrate tri-hydrate ($Cu(NO_3)_2 3H_2O$, 99%), Congo red (CR) dye, sodium hydroxide (99%), and hydrochloric acid (37%) have been acquired from Merck.

2.2. Characterization

Optical absorption was measured using UV-visible absorption spectra in the range 290–650 nm; the spectra were measured *via* single-beam spectroscopy (EMCLAB GmbH GERMANY). X-ray diffraction (XRD) was utilized to examine material crystallinity, structure and phase purity. The analysis was performed utilizing a PAN analytical X′Pert PRO, scanning at 1° min^{-1} throughout a 2θ range of (5° to 75°), utilizing radiation of Cu Kα (λ = 1.540 Å). The chemical structure of the resultant nanostructures was examined with an EDX inside the SEM system. EDX reliant on the interactions among the sample and X-ray excitation is utilized for chemical and elemental analyses. The size and surface appearance of the synthesized nanoparticles have been examined using field emission scanning electron microscopy (FE-SEM). The surface characteristics and purity of nanoparticles were evaluated by obtaining Fourier transform infrared (FT-IR) spectra utilizing a PerkinElmer (RX1) FT-IR spectrometer within a range of 400–4000 cm^{-1}. The zeta potential technique (Zetasizer Nano ZS, Malvern) has been utilized to determine and identify the stability of CuO nanoparticles. The specific surface area (SSA) of the produced CuO nanoparticles, following calcination, ultrasonic treatment, and subsequent air drying, has been determined using a 5 point N_2 adsorption isotherm by BET analysis, measured using a Micromeritics TriStar II Plus equipped with Microactive software and the Microtrac Bel Cor BElSORP-Mini. Prior to the analysis, the sample powder underwent drying for 4 hours at 150 °C in synthetic air.

2.3. Plant collection

M. sylvestris leaves were plucked and collected from the Bira kapra village-Zebar area/Duhok–Kurdistan region of Iraq during the Month of March 2024. All the solutions were produced with deionized water.

2.4. *M. sylvestris* leaf extract preparation

M. sylvestris leaves were thoroughly rinsed and washed using deionized water multiple times to eliminate contaminants and dust particles, followed by air drying at room temperature in a dark environment. 10 grams of the dried leaves were finely powdered and mixed in 100 mL of deionized water. The solution was then further heated for one hour at 75 °C with stirring. After that, the extract was filtered and centrifuged to proceed with the next steps.

2.5. Phytochemical screening

To carry out the phytochemical investigation of the plant extract, several chemical tests were performed for testing the extract, according to the following standards.[54–61]

2.6. CuO nanoparticle synthesis

The fabrication process of CuO nanoparticles was conducted utilizing a precipitation approach based on the previous methods with minor modifications.[62] In a standard procedure, a stoichiometric amount of copper ion precursor (0.1 mol L^{-1}) is mixed with 100 mL of deionized water, and then the solution is heated under magnetic stirring at 65 °C; after 30 min, the plant extract of *M. sylvestris* (20 mL) is added dropwise to the solution and further heated for 30 min; the solution color changes from blue to brown-green. At this temperature, an aqueous solution of sodium hydroxide (NaOH, 1 mol L^{-1}) was dropwise added until the pH reached 12; a suspended precipitate of nanoparticles was formed; the solution was stirred continuously for 1 hour. The precipitate was then centrifuged, washed and rinsed many times with absolute solvent of ethanol and deionized water. The precipitate was oven-dried for 12 hours to remove moisture and residual plant extract. To promote oxide formation and enhance crystallinity, the dried sample was then calcined at 450 °C for 2 hours at a heating rate of 4 °C min^{-1}.

2.7. Batch adsorption experiments

Comparative research was done to assess the effectiveness of synthesized CuO nanoparticles for CR dye removal from aqueous solutions. Batch experiments have been performed to determine and evaluate the impacts of different variables, including initial CR dye concentration (ranging from 4 to 12 mg L^{-1}), pH (4, 5, 6, 7, 9, and 12), contact time (5–60 min), temperature (20, 25, 30, 35, and 40 °C), and adsorbent dose (0.01–0.03 g). For each experiment, a 100 mL Erlenmeyer flask was employed, containing 30 mL of CR solution with specified concentrations, pH levels, temperatures, adsorbent doses, and contact times. The solution was then stirred consistently at a rate of 300 rpm using a digital magnetic hotplate stirrer. At regular intervals samples were collected, centrifuged for 2 min at 8000 rpm, and the absorbance of the supernatant was checked and measured. The adsorption capacity was then subsequently determined *via* the formula, q_e:

$$q_e = \frac{(C_0 - C_e) \times V}{m} \quad (1)$$

The ultimate and initial concentrations of the CR dye in the solution (C_e and C_0, respectively) are expressed in (mg L^{-1}) and are used to determine solution volume (V) in liters and mass (m) of adsorbents in grams.[63]

Experimental equilibrium data have been analyzed utilizing the models of Freundlich and Langmuir isotherms. The Langmuir model is articulated as shown in the following equations:[64–66]

$$\frac{C_e}{q_e} = \frac{1}{bq_{max}} + \frac{1}{b_{max}}C_e \quad (2)$$

$$R_L = 1/(1 + bC_0) \quad (3)$$

In this context, q_{max} is the maximum adsorption (mg g^{-1}), q_e represents adsorbate solid phase concentration at equilibrium, b denotes the Langmuir constant (L mg^{-1}), which corrosponds to the adsorption energy, and C_e denotes the concentration equilibrium of the CR dye (mg L^{-1}). The maximum adsorption and Langmuir constant might be acquired by graphing C_e/q_e against C_e, with the intercept representing $1/bq_{max}$. The R_L value denotes the isotherm shape as unfavorable ($R_L > 1$), favorable ($0 < R_L < 1$), linear ($R_L = 1$), or irreversible ($R_L = 0$).[67]

The isotherm model of Freundlich is an empirical equation utilized for heterogeneous surfaces or surfaces with varying affinities. The logarithmic representation of the isotherm model of Freundlich is articulated as:[68]

$$\ln q_e = \ln K_f + \frac{1}{n}\ln C_e \quad (4)$$

where K_f and n indicate the adsorption capacity and intensity, with K_f serving as a constant for adsorption efficiency, and $1/n$ is the slope which varies from zero to one; this reflects the degree of surface heterogeneity, where values approaching zero suggest more heterogeneity. A ratio of $1/n$ less than 1 implies a typical Langmuir isotherm, where a value larger than 1 signifies cooperative adsorption. K_f and n may be ascertained by graphing $\ln q_e$ *vs.* $\ln C_e$.

The adsorption kinetics were examined utilizing the models: pseudo-first order and pseudo-second order. The pseudo-first order model is articulated using the Lagergren equation, which determines the rate of the adsorption constant (k_1) from the plot of $\ln(q_e - q_t)$ *vs.* t, in which q_t and q_e indicate the adsorbed quantities at time t and at equilibrium.[69]

$$\ln(q_e - q_t) = \ln q_e - k_1 t \quad (5)$$

The pseudo-second order model, on the other hand, calculates the second order rate constant (k_2) from the linear plot of t/q_t *vs.* t.

$$\frac{t}{q_t} = \frac{1}{k_2 q_e} + \frac{1}{q_e}t \quad (6)$$

The intra-particle diffusion model calculates the diffusion rate constant (k_{id}) from the linear plot of (q_t) *versus* ($\sqrt{t}$), based on the Weber–Morris equation:[70]

$$q_t = k_{id} \cdot t^{1/2} + C \quad (7)$$

Thermodynamic parameters, involving entropy (ΔS°), enthalpy (ΔH°), and free energy (ΔG°), were computed utilizing equations that incorporate the equilibrium constant (K_c), absolute temperature (T), and the universal gas constant (R). The parameters were derived using the $\ln K_c$ against $1/T$ plot, with the slope indicating DH°/R and the intercept denoting DS°/R.[71]

$$\ln K_c = -\frac{\Delta H^\circ}{RT} + \frac{\Delta S^\circ}{R} \quad (8)$$

$$\Delta G^\circ = -RT \ln K_c \quad (9)$$

$$K_c = \frac{q_e}{C_e} \quad (10)$$

2.8. pH at the point of zero charge (pHpzc)

The point of zero charge (pHpzc) is defined as the pH at which the surface of the adsorbent carries no net electrical charge, meaning the concentrations of positive and negative surface charges are equal. The pHpzc of CuO nanoparticles was determined using the pH drift method. A series of 0.005 mol L^{-1} NaCl solutions were adjusted to initial pH values ranging from 2 to 12 using either HCl or NaOH (0.1 M). Then, 0.03 g of CuO nanoparticles was added to 20 mL of each solution in Erlenmeyer flasks and allowed to equilibrate at room temperature for 48 hours. After stabilization, the final pH of each solution was then recorded. The difference between the initial and final pH values (eqn (11)) was plotted against the initial pH. The pHpzc was identified as the point where ΔpH equals zero, in other words, where the curve intersects the x-axis.[72,73]

$$\Delta pH = pH_f - pH_i \quad (11)$$

2.9. Adsorbent regeneration process

Practical adsorption requires an adsorbent's ability to be renewed and reused with optimal efficiency. To test the feasibility of regenerating CuO nanoparticles, 50 mL of the CR dye

with 4 ppm concentration was brought into contact with 0.1 g for half-an-hour time duration at 20 °C temperature and pH 7.0.'' to ''50 mL of the CR dye with 4 ppm concentration was mixed with 0.1 g of CuO nanoparticles for half-an-hour at 20 °C and pH 7.0. UV-vis spectroscopy was utilized to quantify the adsorbed CR dye. The adsorbent was washed with 50% ethanol (v/v) solution in deionized water five times and tested for CR dye concentration utilizing a UV-vis spectrophotometer. Five adsorption–desorption cycles were done. The following equation was used to calculate the regeneration percentage (Re%).[74]

$$\% \text{ Re} = \frac{V \cdot C_M}{M \cdot q_e} \times 100 \quad (12)$$

3. Results and discussion

3.1. Phytochemical analysis of the *M. sylvestris* leaf extract

An examination of phytochemicals was carried out to determine the bioactive components found in *M. sylvestris* leaves using several chemical tests as shown in Fig. 1 and to understand the relationship among these phytochemicals and their biological activity, which is crucial, particularly for applications such as green synthesis of nanoparticles. The extract was essential for reducing and stabilizing the nanoparticles. Polyphenolic metabolites (flavonoids, phenolics, and tannins) in the *M. sylvestris* extract are suggested to serve as primary reducing agents for Cu^{2+} ions through hydroxyl and carbonyl functional groups, whilst proteins, amino acids, and saponins are anticipated to function as capping and stabilizing agents. This cooperative approach facilitates both the nucleation and stability of CuO nanoparticles, in accordance with previous research on plant-mediated green synthesis.[75,76] The principal bioactive components discovered in the extract are summarized in Table 1. These results closely align with current research,[50] further affirming the consistency and potential of the *M. sylvestris* plant in environmentally sustainable nanotechnology applications.

Table 1 Phytochemical test results

Active constituent	Chemical test	Results	Indication	Ref.
Flavonoid	Lead acetate	++ve	Yellow ppt	54
Carbohydrate	Molish	+ve	Violet ring	55
Alkaloid	Hager	−ve	No change	56
Phenolic	Lead acetate	++ve	Yellow ppt	57
Glycoside	Benedict	+ve	Reddish ppt	58
Tannin	Braymer	+ve	Brownish-green	59
Protein	Biuret	+ve	Purple color	60
Amino acid	Ninhydrin	+ve	Violet green color	60
Saponin	Foam	+ve	Foam formation	61

3.2. Characterization of CuO nanoparticles

The morphological characteristics of synthesized CuO nanoparticles have been assessed utilizing FE-SEM. The nanoparticles have a granular and distinct spherical shape, as seen in the FE SEM picture in Fig. 2A and B. The particles seem to be uniformly distributed with little aggregation, which is prevalent in nanoparticles owing to abundant surface energy, electrostatic attraction and also the incorporation of biological components in the process of synthesis. However, it should be noted that some degree of aggregation observed in the SEM images may also result from the sample drying process during SEM preparation.[77,78] The uniform size of nanoparticles ranges from 26 nm to 41 nm, indicating good control of parameters over the process of synthesis. This nanoscale uniformity and spherical shape align with typical results of green synthesis, where plant based reducing agents affect particle nucleation and stabilization.[79]

The EDX mapping and spectrum validate the effective production of synthesized CuO nanoparticles, with some additional elements probably introduced as contaminants during sample preparation or analysis. Fig. 2C shows strong peaks belonging to the copper element and oxygen. Quantitative analysis reveals the atomic percentages of Cu of approximately 26.2% and O around 46.3, consistent with expected stoichiometry and signifying the synthesis of CuO nanoparticles. Carbon was present in minimal quantities as a result of using the extract of *M. sylvestris* leaves in the synthesis process. A comparable spectrum is seen for the *Calotrupis G.* plant leaf extract[80] and *Moringa oleifera* leaf extract[81] The EDX spectrum was verified using the EDX mapping figure, which is essential for ensuring consistent material properties. As shown in Fig. 2D, the uniformity distribution signifies the successful synthesis of CuO nanoparticles.

The XRD spectrum of synthesized CuO nanoparticles reveals a series of diffraction peaks, verifying their crystalline structure. The identified peaks align with the monoclinic CuO phase (JCPDS 96-110-0029).[82,83] Significant peaks appeared at 2θ

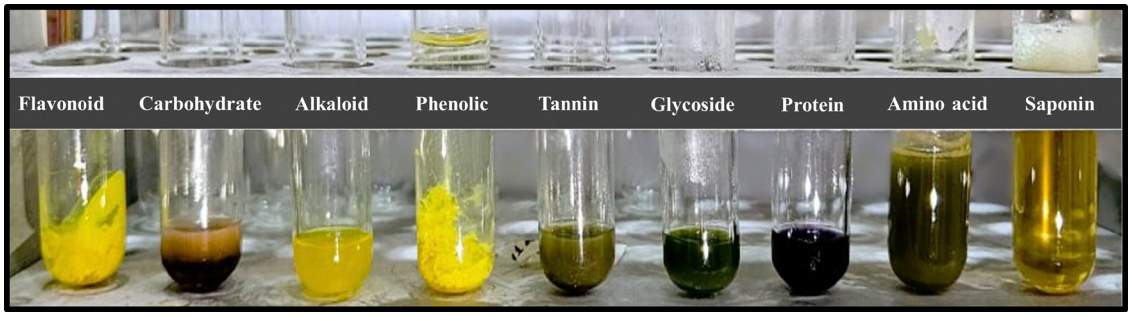

Fig. 1 Image showing the phytochemical test screening results.

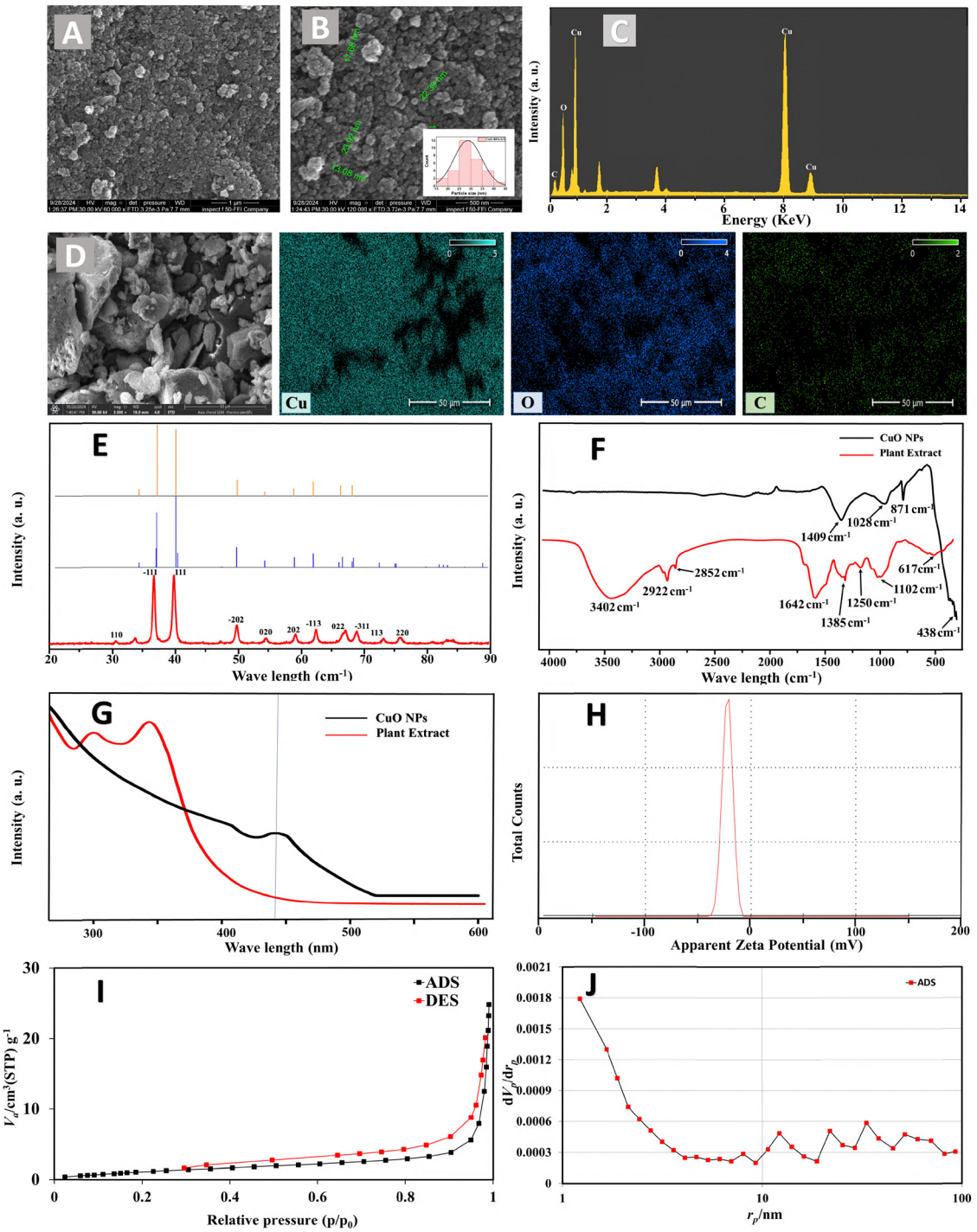

Fig. 2 (A) and (B) FE-SEM images of CuO NPs. (C) and (D) EDX spectrum and mapping spectrum of CuO NPs. (E) XRD pattern of the CuO NPs. (F) FTIR spectra of the *Malva sylvestris* extract and synthesized CuO NPs. (G) UV-visible spectrum of the plant extract and CuO NPs. (H) Zeta potential analysis of CuO NPs. (I) and (J) BET analysis of CuO NPs.

values of 32.69°, 35.75°, 38.92°, and 49.06°, corresponding to the 110, −111, 111, and −202 planes, respectively, Fig. 2E. The pattern in the figure shows diffraction peaks of the synthesized nanoparticles and their corresponding crystalline phases; the red curve represents the XRD pattern of the CuO nanoparticle, whereas the overlaid lines correspond to reference diffraction patterns for phase identification. The peak distribution and positions match well with monoclinic CuO (tenorite) as indicated by the blue reference line peak, confirming the successful synthesis of the expected crystalline phase. Lattice parameters for biosynthesized nanoparticles were a = 4.653, b = 3.410, and c = 5.108. These findings align with prior publications on CuO

Table 2 XRD peak parameters, FWHM, and crystallite size of CuO nanoparticles calculated using the Scherrer equation

No.	*hkl*	2θ (°)	FWHM (°2θ)	B (°)	cos(θ)	β (radians)	D (Å)
1	110	32.7	0.5486	0.0096	0.9595	0.0096	15.10
2	−111	35.7	0.4131	0.0072	0.9518	0.0072	20.22
3	111	38.9	0.51	0.0089	0.9429	0.0089	16.53
4	−202	49.1	0.477	0.0083	0.9095	0.0083	18.32
5	020	53.7	0.5865	0.0102	0.8921	0.0102	15.19
6	202	58.7	0.4879	0.0085	0.8715	0.0085	18.70
7	−113	61.9	0.4193	0.0073	0.8575	0.0073	22.11
8	022	66.1	0.6897	0.0120	0.8381	0.0120	13.75
9	−311	66.7	0.4385	0.0076	0.8352	0.0077	21.70
10	113	68.5	0.6486	0.0113	0.8265	0.0113	14.83

nanoparticles synthesis.[83–85] The average crystallite size of the biosynthesized CuO nanoparticles, calculated from the Debye–Scherrer equation applied to the main diffraction peaks, was ~17.7 nm (Table 2). This value is smaller than the particle size observed in FE-SEM images (26–41 nm). Such a difference is commonly reported in nanomaterials studies, since XRD estimates the size of individual crystallites, whereas SEM reflects the overall particle size, which may consist of multiple crystallites.[86]

The FTIR spectra of *M. sylvestris* leaf extract and synthesized CuO nanoparticles are presented in Fig. 2F, revealing characteristic bands that confirm the presence of biomolecules involved in nanoparticle formation and surface functionalization.[87] In the plant extract spectrum, a broad band at 3402 cm^{-1} is attributed to O–H stretching vibrations, indicating hydroxyl groups from polyphenols or alcohols. Peaks at 2922 cm^{-1} and 2852 cm^{-1} are assigned to asymmetric and symmetric C–H stretching of aliphatic $-CH_2$ groups, typically found in fatty acids and phytosterols.[88]

The fingerprint region shows absorptions at 1642 cm^{-1} (C═C stretching in aromatic rings), 1385 cm^{-1} (O–H bending), and 1250 cm^{-1} (C–O stretching), which are consistent with flavonoids and phenolic compounds. Additional bands at 1102 cm^{-1} and 617 cm^{-1} correspond to C–O–C and C–H bending, respectively, further supporting the presence of secondary metabolites like tannins and glycosides, which likely acted as reducing and stabilizing agents during synthesis.[88,89]

For the CuO nanoparticles, a prominent peak at 438 cm^{-1} confirms the formation of Cu–O bonds, characteristic of CuO lattice vibrations. In addition, weaker absorptions at 1409 cm^{-1} (N–H bending/C–N stretching or symmetric COO^- stretching), 1028 cm^{-1} (C–O–C/C–O stretching of glycosidic or phenolic residues), and 871 cm^{-1} (aromatic C–H out-of-plane bending) indicate that plant-derived functional groups remain attached to the nanoparticle surface. These residual biomolecular features suggest the presence of a thin phytochemical capping layer that enhances colloidal stability and adsorption activity. Such assignments are consistent with earlier reports on CuO nanoparticles synthesized using plant extracts.[90–92] The FTIR spectra further confirm the presence of phytochemical residues (–OH, –C═O, and $-NH_2$ groups) on the CuO nanoparticle surface, derived from the *M. sylvestris* extract. These biomolecules can provide additional adsorption-active moieties, enhancing dye interaction through hydrogen bonding, electrostatic interactions, and π–π stacking, thereby increasing adsorption capacity compared to chemically synthesized CuO.[93,94] Although calcination at 450 °C removes most of the plant extract, the EDX and FTIR spectra indicate that only a minor fraction of thermally stable phytochemical residues remains on the CuO surface, providing additional functional groups that contribute to dye adsorption.

The optical characteristics of CuO nanoparticles are examined using UV-visible spectroscopy. The conversion of the copper nitrate precursor to CuO nanoparticles was verified by analyzing the UV-vis spectra between 250 and 600 nm for both the plant extract and the resultant product as shown in Fig. 2G. As anticipated, CuO nanoparticles exhibit a peak within the range of 400 to 500 nm, namely at 442 nm, attributable to the characteristic absorption of nanoparticles, which can be easily distinguished from the spectrum of the plant extract.[95]

The stability and dispersion of CuO nanoparticles have been investigated using the zeta potential technique; as shown in Fig. 2H, the average zeta potential value is −25 mv, indicating their good colloidal characteristics, enhanced disparity and prolonged stability.[81] The narrow peak distribution indicates a homogeneous particle population with consistent surface characteristics. This outcome indicates the significant stability of CuO nanoparticles and demonstrates durable electrostatic repulsion force between the nanoparticles, which decreases aggregation.[96]

BET was utilized to calculate the pore volume, size, and surface area of synthesized CuO nanoparticles. An illustration of a type IV isotherm characterized by the H-3 hysteresis loop, as per IUPAC classification, Fig. 2I and J, revealed a mesoporous structure with a significant surface area for CuO nanoparticles, indicating their good potential for the adsorption process. The nanoparticle, based on BET data, exhibits significant pore uptake and an ample surface area. The N_2 adsorption isotherm of the nanoparticles exhibited a BET surface specific area (SSA) of approximately 5.3 $m^2\ g^{-1}$, a mean pore size of 27.4 nm, and a pore volume of 0.0364 $cm^3\ g^{-1}$.

A separate investigation revealed that the BET surface area of synthesized CuO nanoparticles using the simple precipitation method was 1.7 $m^2\ g^{-1}$, with sizes ranging from 140 to 180 nm.[97] Another research conducted by Dorner *et al.* reported that the BET surface area of sol–gel produced CuO nanoparticles was 16 $m^2\ g^{-1}$, and the size range was 100–140 nm.[98]

3.3. Adsorption study

3.3.1. Effect of the initial concentration. The influence of CR dye concentration on the adsorption process was investigated using different concentrations of 4, 6, 8, 10, 12, and 14 mg L^{-1}, while maintaining constant variables including contact time (60 min), pH (7.0), temperature (20 °C), and nanoparticle dose (0.01 g to 10 mL of CR dye solution). Fig. 3A illustrates that the CR dye removal capability increased as the initial dye concentration decreased. The higher absorption of the CR dye at lower concentrations might be attributed to the higher active site availability on the adsorbent surface for

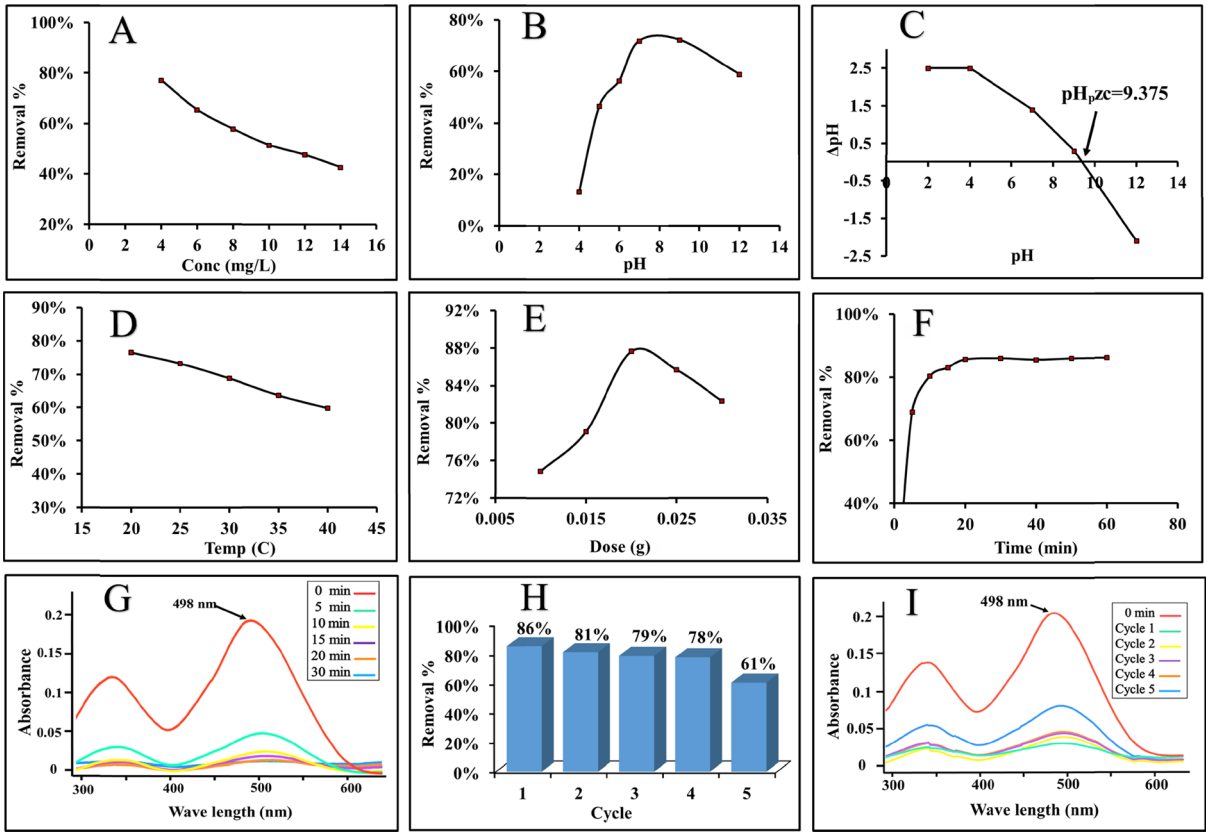

Fig. 3 The influence of various parameters of CuO NPs on the absorbance and removal of the CR dye. (A) CR dye conc., (B) pH, (C) point of zero charge (pHpzc) analysis, (D) temperature, (E) catalytic dose, (F) initial time, (G) absorbance of the CR dye at different times, (H) the recyclability of CuO NPs for the removal of the CR dye and (I) the absorbance of the CR dye at different cycles.

the adsorption of CR molecules. Conversely, at elevated concentrations, these active sites may become quickly saturated, resulting in a limited capacity to adsorb additional CR molecules.[99] For further experiments, a concentration of 4 mg L^{-1} of CR dye was utilized as the best setting for the adsorption process which is essential for maximizing removal efficiency.

3.3.2. Effect of pH. The impact of solution pH is essential in the process of adsorption, since it affects the ionization state of the target molecules and characteristic surface of the adsorbent's functional groups. The protonation degree of the active functional groups with acid–base properties in solution is controlled by the pH. The influence of pH has been investigated, while maintaining constant parameters including CR dye concentration (4 ppm), contact time (60 min), temperature (20 °C), and adsorbent dose (0.01 g to 10 mL of CR dye solution), Various pH levels, including 4.0, 5.0, 6.0, 7.0, 9.0, and 11.0, have been studied. The solution pH was modified using 0.1 M solutions of NaOH and HCl. The outcomes, as illustrated in Fig. 3B, revealed that the highest removal capacity of CuO nanoparticles occurred within pH 7.0 and 9.0. Significantly, by reducing the pH of the solution below 5.0 (by adding HCl acid) the colour of the CR dye changes from red to purple; the CR dye becomes very sensitive. The primary peak of the CR dye seen at λ 488–500 nm attempts to move towards the higher wavelength nearly reaching 537 nm at pH 4.0 and 595 nm at pH 2.0 respectively. The bathochromic shift and reduction in the intensity of the CR monomer are ascribed to the partial self-association of CR monomers.[100] Notably, the removal capacity showed low efficiency in acidic medium at pH 5 and 6, but it reached the maximum in neutral medium at pH 7.0 and moderate base at pH 9.0 and started to decrease under strong base condition at pH 12.0. In accordance with these findings, pH 7.0 was chosen as the best condition for the process of adsorption, since the majority of water bodies exhibit a pH range of 6.5 to 7.5; moreover, it provides a neutral environment and reduces possible unpredictability in the mechanism.[101] The neutral pH was chosen in the subsequent experiment to enhance adsorption efficacy and to obtain deeper insight into the underlying adsorption mechanism.

The pHpzc of the synthesized CuO nanoparticles was determined using the pH drift method. As shown in Fig. 3C, based on the ΔpH *vs.* initial pH plot, the pHpzc was identified at approximately pH 9.4. This implies that the CuO surface is positively charged below pH 9.4, which enhances electrostatic attraction with the anionic CR dye, explaining the observed maximum adsorption at pH 7.[72,73] While zeta potential after adsorption was not measured, it is likely that surface interactions with dye molecules shift the surface charge slightly, as commonly reported in similar systems.[102] Although the measured zeta potential was negative (–25 mV), this reflects the

effective charge in suspension influenced by phytochemical residues and the ionic environment, whereas the intrinsic oxide surface charge (pHpzc ≈ 9.4) governs the electrostatic attraction with Congo red at pH 7. Therefore, there is no contradiction between the zeta potential value and the observed adsorption behavior.

It should be noted that under strongly acidic conditions, CuO nanoparticles may release small amounts of Cu^{2+}, which could affect adsorption behavior; therefore, maintaining near neutral pH is preferable for practical applications.[103]

3.3.3. Effect of temperature. The impact of temperature on the adsorption process of the CR dye has been examined at various temperatures (20, 25, 30, 35, and 40 °C). The other parameters were kept constant, including the CR dye concentration (4 ppm), pH (7.0), time (60 min), and nanoparticle dose (0.01 g in 10 mL of CR dye solution). As shown in Fig. 3D, the removal capacity reached a maximum at a temperature of 20 °C, which is likely due to stronger physical adsorption and favorable adsorption interaction. However, the removal capacity then started to decrease gradually as the temperature increased and reached a minimum at 40 °C; this is possibly due to weakened adsorption forces, desorption of CR molecules and increased thermal agitation. This suggests that the process of adsorption is exothermic.[104] Thus, 20 °C is the optimal temperature, which is important for maximizing removal capacity; this temperature is selected as the best setting for the adsorption process.

3.3.4. Effect of nanoparticle dose. The impact of catalytic dose of CuO nanoparticles on the CR dye has been examined using different dose amounts including 0.01, 0.015, 0.02, 0.025, and 0.03 g per 10 mL of CR dye, fixing other parameters including the initial concentration of CR dye (4 ppm), pH (7.0), temperature (20 °C), and contact duration (60 min). The data as shown in Fig. 3E revealed that the removal percentage of the CR dye rises from 75% to 85% at 0.01 and 0.02 g respectively. This is attributable to the enhanced accessibility of the adsorbent sites at higher doses of the adsorbent. Beyond this optimal dose, the removal capacity begins to decline slightly; the best explanation is agglomeration possibility, which reduces the effective surface area and limits CR dye accessibility to active spots. Thus 0.02 g of the catalyst is the optimal catalytic dose, which is essential for maximizing removal capacity; this dose is selected as the best setting for the adsorption process.

3.3.5. Effect of the initial time. To find out the maximum absorbance capacity of the CR dye at a given time, the influence of time is examined within 60 min., while fixing all other parameters including the concentration of CR dye (4 ppm), pH (7.0), temperature (20 °C), and dose concentration of catalyst (0.02 g per 10 mL of CR dye solution). The absorbance capacity reaches its maximum after only 30 min, as seen in Fig. 3F; the removal capacity increases rapidly within the first 10–15 min, reaching ∼80%, this indicates a fast adsorption rate initially owing to abundant active sites on the nanoparticle surface. The adsorption starts to slow down and the removal efficiency plateaus, suggesting that equilibrium is achieved by around 20–30 min. Beyond this point, no significant improvement in removal efficiency is observed, as the adsorption sites are mostly saturated. Consequently, as shown in Fig. 3G a contact period of 30 min was determined to be optimal for achieving optimum removal efficiency.

3.3.6. Regeneration results. The regeneration of the CuO nanoparticles has been investigated during five cycles *via* reusing the CuO nanoparticles for fresh solution of the CR dye. As illustrated in Fig. 3H and I, there is no doubt that the adsorption capacity of the adsorbent is maximum during its first cycle. A probable desorption mechanism involves disruption of hydrogen bonding and weakening of electrostatic interactions by ethanol, which lowers the binding affinity of CR dye molecules on the CuO surface.[105] After the use of the adsorbent, a considerable fraction of sites engage in adsorption and are occupied by the molecules of the adsorbate, resulting in the adsorption capacity of the adsorbent being reduced. The regeneration process is an effective technique for the repeated use of the adsorbent. A regenerable adsorbent is both efficient and economical.

3.3.7. Adsorption isotherm. The adsorption data analysis is essential for assessing the adsorption capability of the nanoparticles. Reaching equilibrium, the adsorbate concentration in the solution maintains a dynamic balance with that at the nanoparticle interface, leading to a stable solution concentration.[106]

The experimental results for CR dye adsorption on CuO nanoparticles were accurately modeled using the Langmuir equation, with the regression coefficient (R^2) equal to 0.9943, Fig. 4A. The Langmuir constants K_L and R_L were determined to be 0.6415 L mg^{-1} and 0.2804, respectively. R_L indicates that the adsorption process is favorable. The q_{max} was determined to be 6.9903 mg g^{-1}. Moreover, the Freundlich model demonstrated a linear fit with a coefficient of determination (R^2) of 0.9925, Fig. 4B, which is higher than that of the Langmuir model. The Freundlich correlation gives values of $1/n$ as 0.325 and K_f as 3.0688 mg g^{-1}. A $1/n$ value below 0.5 indicates favorable adsorption and significant surface heterogeneity, suggesting that multiple classes of active sites are involved in CR uptake.[107]

To contrast the fitted isotherm models, it is evident from Table 3 that both Langmuir and Freundlich isotherm models provide the optimal fit determined by the coefficient of determination of R^2.

3.3.8. Adsorption kinetics. The adsorption rate of the CR dye on CuO nanoparticles was initially elevated but gradually diminished until equilibrium was reached. After 30 min, the rate of adsorption increased and the highest adsorption was seen; this is defined as the equilibrium time. The kinetics of dye removal are essential factors for assessing adsorption dynamics. Both models, pseudo-first order and pseudo-second order, are revealed in Fig. 4C and D. These models were utilized to correlate the findings and analyze the kinetics of CR dye elimination on CuO nanoparticles.[108]

The fit of different kinetic models to the experimental data was investigated using the determination coefficient (R^2) and computed adsorption capacities, as presented in Table 3. The higher R^2 values revealed that the adsorption of the CR dye is

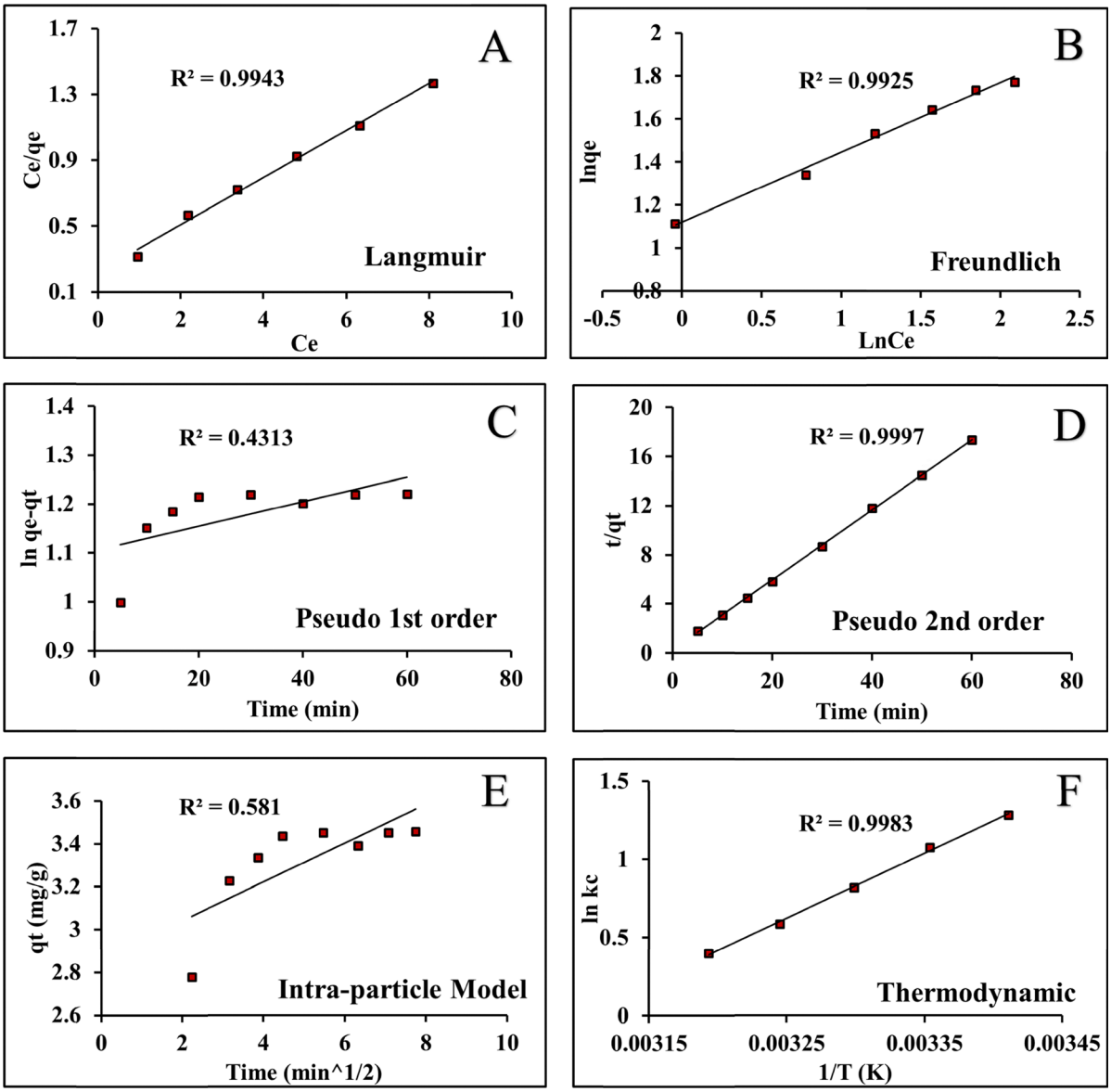

Fig. 4 (A) The line plot of the Langmuir isotherm (solid lines are linear fittings). (B) The line plot of the Freundlich isotherm (solid lines are linear fittings). (C) Pseudo-first-order kinetic model (solid lines are linear fittings). (D) Pseudo-second-order kinetic model (solid lines are linear fittings). (E) Intra-particle diffusion model. (F) Thermodynamic parameters for adsorption of the CR dye onto CuO nanoparticles with time dependency at different temperatures (20, 25, 30, 35, 40, and 45 °C).

more accurately expressed in the pseudo-second-order model. This model's predicted adsorption capacity closely matches the observed experimental values, unlike the pseudo-first-order model. The data indicate that the adsorption process likely entails chemical interactions, including bonding forces or the exchange of ions and electrons, between the CR dye molecules and the CuO nanoparticles.[106]

In addition to the pseudo-first order and pseudo-second order models, the adsorption mechanism was further examined using the intra-particle diffusion model (Weber–Morris plot). As shown in Fig. 4E, the plot of q_t *versus* $t^{1/2}$ showed a multilinear relationship with a non-zero intercept. This indicates that while intra-particle diffusion contributes to the overall rate of CR dye adsorption, it is not the sole rate-limiting step. The observed intercept suggests the presence of boundary layer effects during the initial phase, followed by gradual diffusion into the internal pores of the CuO nanoparticles. These findings support a multi-step adsorption process involving both surface adsorption and intra-particle transport, in agreement with prior studies.[109]

3.3.9. Thermodynamic studies. The impact of temperature on adsorption is essential for practical applications of the adsorbent, utilized at 20, 25, 30, 35, 40, and 45 °C, Fig. 4F.

The adsorption capacity of CuO nanoparticles for the CR dye was diminished as temperature increased from 20 to 45 °C, suggesting that the adsorption of the CR dye onto the CuO nanoparticles is an exothermic process. The calculated thermodynamic parameter findings are shown in Table 3. Physisorption

Table 3 Isotherm results for CR dye adsorption onto CuO NPs (Langmuir and Freundlich). Kinetic results for CR dye adsorption onto CuO NPs: pseudo-first order, pseudo-second order and intra-particle diffusion models. Thermodynamic parameters including standard enthalpy ΔH°, entropy ΔS°, and free energy changes ΔG° for CR dye adsorption

Model	Parameter	Value	Model	Parameter	Value
Langmuir isotherm	q_{max} (mg g^{-1})	6.9903	Freundlich isotherm	q_{max} (mg g^{-1})	3.0688
	K_L (L mg^{-1})	0.6415		K_f	3.0688
	R_L	0.2804		$1/n$	0.3250
	R^2	0.9943		R^2	0.9925
1st order kinetics	q_e (mg g^{-1})	3.02	2nd order kinetics	q_e (mg g^{-1})	3.51
	K_1 (min^{-1})	0.00252		K_2 (g mg^{-1} min^{-1})	0.3278
	R^2	0.4313		R^2	0.9997
Intra-particle diffusion	k_{id} (mg g^{-1} min$^{-1/2}$)	0.0906		Intercept C	2.858
	R^2	0.5823			
Thermodynamics	ΔH° (kJ mol^{-1})	−34.35	ΔS° (J mol^{-1} K^{-1})	−106.46	
	ΔG° (kJ mol^{-1}) at 293.15 K	−3.1225	298.15 K	−2.6656	
	303.15 K	−2.0634	308.15 K	−1.5105	
	313.15 K	−1.0387			

alters free energy within the range of 20 to 0 kJ mol^{-1}, while chemisorption modifies free energy within the range of 80 to 400 kJ mol^{-1}. The negative results of ΔG° and ΔH° indicate that the process of adsorption is both spontaneous and exothermic. The reaction is verified to be more probable at lower temperature. The negative ΔS° indicates a reduction randomness (orderliness) at the CuO nanoparticles.[104,110]

3.3.10. Mechanism of adsorption. The mechanism of adsorption of the CR dye onto CuO nanoparticles utilizing *M. sylvestris* leaf extract follows both monolayer and multilayer adsorption models, as confirmed by both isotherm models, Langmuir and Freundlich. This suggests that CuO nanoparticles exhibit a variety of adsorption sites with different affinities for CR dye molecules. The adsorption also adheres to pseudo-second order kinetics, indicating a chemisorption-dominated process, wherein the adsorption rate is dependent upon the available active sites of CuO nanoparticles rather than only on CR dye concentration. This indicates strong interactions, including complexation, hydrogen bonding, and electrostatic attraction, between CuO nanoparticles and CR dye molecules. Fig. 5 presents FE-SEM images showing the surface morphology of CuO nanoparticles before and after the adsorption process. Fig. 5A, captured prior to adsorption, displays well-dispersed, highly porous, and uniformly distributed CuO nanoparticles, providing an extensive surface area for the process of CR dye adsorption. Conversely, as shown in Fig. 5B (after adsorption) demonstrates a notable change in surface texture, indicating that the nanoparticles are coated and aggregated as a result of CR dye molecule adsorption. This morphological modification indicates effective adsorption, with CR dye molecules occupying the active sites on the surface of CuO nanoparticles, resulting in a denser and rougher structure.

To elucidate the adsorption mechanism, a schematic diagram as shown in Fig. 6 illustrates how CR dye molecules interact with CuO nanoparticles through electrostatic attraction between anionic sulfonate groups of CR and positively charged CuO surfaces at pH < pHpzc, hydrogen bonding between CR functional groups and CuO surface hydroxyls, and π–π stacking among aromatic rings. It is further possible that π–π stacking occurs not only directly with phytochemical residues on the

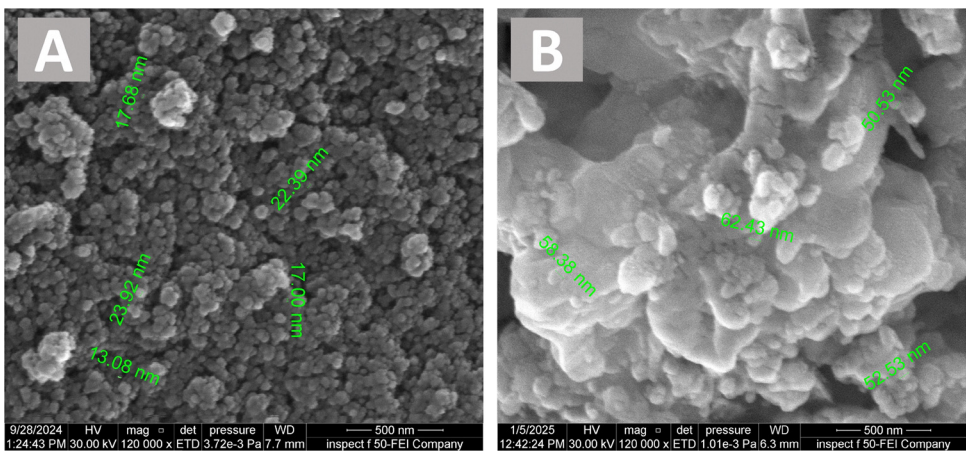

Fig. 5 FE-SEM images of CuO NPs (A) before adsorption and (B) after adsorption.

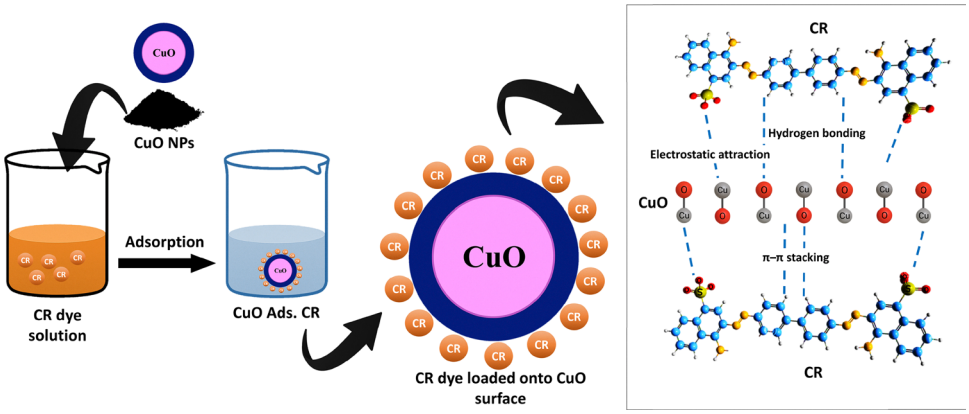

Fig. 6 Schematic illustration of the adsorption mechanism of the CR dye onto CuO nanoparticles.

CuO surface but also among adsorbed CR molecules, contributing to multilayer adsorption as suggested by the Freundlich model. These synergistic non-covalent interactions align with the observed pH-dependent adsorption behavior, confirming that electrostatic forces predominantly govern the initial adsorption process.[111–113]

3.3.11. Comparative evaluation of adsorbent performance. To better understand the significance of our results, we compared the performance of our nanoparticles with several other Cu-based adsorbents reported in the literature, as shown in Table 4. While some materials such as CuO/Fe_2O_3 bimetallic nanoparticles exhibited higher removal efficiencies (up to 97%) within very short contact times, these systems often involve more complex synthesis routes or costly components. In contrast, our adsorbent achieved a notable 86% removal efficiency in just 30 minutes, without the use of dopants, polymers, or ultrasonic treatment, compared to other green-synthesized CuO-based materials that required up to 120 minutes to reach similar performance; our nanoparticle stands out for its fast kinetics, which is critical for real-time or large-scale water purification applications.

Importantly, the synthesis route based on the *Malva sylvestris* extract offers both environmental and economic advantages, avoiding toxic reagents or high-energy inputs. Taken together, these factors position our CuO nanoparticles as a balanced and practical alternative, combining green synthesis, solid efficiency, and operational simplicity for sustainable dye removal.

4. Conclusions

In conclusion, this study successfully demonstrates the green synthesis of CuO nanoparticles using *M. sylvestris* extract, establishing a cost-effective, eco-friendly, and sustainable approach for nanoparticle production. The resulting CuO nanoparticles exhibited high adsorption efficiency for Congo red dye, with adsorption data fitting well to both Langmuir and Freundlich isotherm models ($R^2 > 0.99$), signifying the coexistence of monolayer and multilayer adsorption. Kinetic modelling revealed pseudo-second-order behaviour ($R^2 = 0.9997$), signifying that chemisorption governs the rate-limiting step. Thermodynamic analysis confirmed the adsorption process to be spontaneous and exothermic ($\Delta H^\circ = -34.35$ kJ mol^{-1}), involving both physical and chemical interactions, as evidenced by the negative entropy change ($\Delta S^\circ = -106.46$ J mol^{-1} K^{-1}). Importantly, the CuO nanoparticles retained over 78% adsorption capacity after four regeneration cycles, underscoring their practical reusability. Collectively, these findings highlight the potential of phyto-synthesized CuO nanoparticles as an efficient, renewable, and economically viable adsorbent for the removal of synthetic dyes from wastewater, supporting their applications in sustainable environmental remediation technologies.

Consent for publication

The authors agreed to publish the manuscript.

Ethics approval and consent to participate

Ethical approval was not required for this study as it did not involve human participants, animals, or sensitive data.

Table 4 Comparison between the published work on adsorption of the CR dye and our work

Nanoparticles	Synthesis	Dye	Adsorbent dose (g L^{-1})	Efficiency	Time (min)	Ref.
CuO	Green synthesis	CR and malachite green	4.0	92.3	80	114
CuO/Fe_2O_3 bimetallic	Green synthesis	CR dye	2.0	97.1	10	115
Mg doped CuO	Green synthesis	CR dye	5.0	81	120	116
ZnO/CuO nanocomposite	Green synthesis	CR dye	2.0	90.1	120	104
CuO	Green synthesis	CR dye	2.0	86	30	Present work

Author contributions

AJM: conceptualization, data curation, formal analysis, investigation, methodology, resources, software, visualisation, writing original draft; KMO: supervision, methodology, writing – review and editing; AKQ: supervision, validation, writing – review and editing.

Conflicts of interest

No potential conflict of interest was reported by the author(s).

Data availability

The datasets used and analysed during the current study are available from the corresponding author upon request.

Acknowledgements

This research received no specific grant from funding agencies. The authors would like to thank the Ministry of Higher Education and Scientific Research in the Kurdistan Region and the University of Zakho and Akre University for applied science for their support.

References

1 N. Joudeh and D. Linke, Nanoparticle classification, physicochemical properties, characterization, and applications: a comprehensive review for biologists, *J. Nanobiotechnol.*, 2022, **20**, 1–29, DOI: **10.1186/s12951-022-01477-8**.

2 Y. Khan, H. Sadia, S. Z. Ali Shah, M. N. Khan, A. A. Shah and N. Ullah, *et al.*, Classification, Synthetic, and Characterization Approaches to Nanoparticles, and Their Applications in Various Fields of Nanotechnology: A Review, *Catalysts*, 2022, **12**, 1386, DOI: **10.3390/catal12111386**.

3 T. Sathish, N. Ahalya, M. Thirunavukkarasu, T. S. Senthil, Z. Hussain and M. I. Haque Siddiqui, *et al.*, A comprehensive review on the novel approaches using nanomaterials for the remediation of soil and water pollution, *Alexandria Eng. J.*, 2024, **86**, 373–385, DOI: **10.1016/j.aej.2023.10.038**.

4 S. S. Mohammed Ameen, M. K. Ibrahim, S. R. Mohammed, M. Chellegui, H. Mohammad-Salim and K. M. Omer, *et al.*, Microwave-Assisted Synthesis of Azo-Chalcone Using Porous MOF Catalysts: Insights from DFT and Molecular Docking, *Catal. Lett.*, 2025, **155**, 284, DOI: **10.1007/s10562-025-05119-0**.

5 S. S. Mohammed Ameen, A. Bedair, M. Hamed, F. R. Mansour and K. M. Omer, Repurposing expired metformin to fluorescent carbon quantum dots for ratiometric and color tonality visual detection of tetracycline with greenness evaluation, *Microchem. J.*, 2024, **207**, 111960, DOI: **10.1016/j.microc.2024.111960**.

6 S. S. Mohammed Ameen, A. Bedair, M. Hamed, F. R. Mansour and K. M. Omer, Recent Advances in Metal–Organic Frameworks as Oxidase Mimics: A Comprehensive Review on Rational Design and Modification for Enhanced Sensing Applications, *ACS Appl. Mater. Interfaces*, 2025, **17**, 110–129, DOI: **10.1021/acsami.4c17397**.

7 S. S. M. Ameen, F. Algethami and K. M. Omer, Magnetic rod-shaped Mn-based MOF as a multi-functional and recyclable platform for dual-mode ratiometric-based nitrite detection, *Microchim. Acta*, 2025, **192**, 1–13.

8 S. C. Baral, P. Maneesha, S. Sen, S. Sen and S. Sen, In *An Introduction to Metal Oxides*. ed Kumar V., Ayoub I., Sharma V., Swart H. C., Springer Nature, Singapore; 2023, pp. 1–34, DOI: **10.1007/978-981-99-5640-1_1**.

9 M. J. Uddin, M. S. Yeasmin, A. A. Muzahid, M. M. Rahman, G. M. M. Rana and T. A. Chowdhury, *et al.*, Morphostructural studies of pure and mixed metal oxide nanoparticles of Cu with Ni and Zn, *Heliyon*, 2024, **10**, e30544, DOI: **10.1016/j.heliyon.2024.e30544**.

10 S. Vijayaram, H. Razafindralambo and Y. Z. Sun, *et al.*, Applications of Green Synthesized Metal Nanoparticles—a Review, *Biol. Trace Elem. Res.*, 2024, **202**, 360–386, DOI: **10.1002/0470862106.ia377**.

11 Z. Alhalili, Metal Oxides Nanoparticles: General Structural Description, Chemical, Physical, and Biological Synthesis Methods, Role in Pesticides and Heavy Metal Removal through Wastewater Treatment, *Molecules*, 2023, **28**, 1–33, DOI: **10.3390/molecules28073086**.

12 R. Kuhn, I. M. Bryant, R. Jensch and J. Böllmann, Applications of Environmental Nanotechnologies in Remediation, Wastewater Treatment, Drinking Water Treatment, and Agriculture, *Appl. Nano*, 2022, **3**, 54–90, DOI: **10.3390/applnano3010005**.

13 M. S. Chavali and M. P. Nikolova, Metal oxide nanoparticles and their applications in nanotechnology, *SN Appl. Sci.*, 2019, **1**, 1–30, DOI: **10.1007/s42452-019-0592-3**.

14 S. S. Mohammed Ameen, F. Algethami and K. M. Omer, Pine needle-derived oxidase-like Mn nanozymes: sustainable nanozyme, scalable synthesis, and visual and colorimetric nitrite detection, *Microchim. Acta*, 2025, **192**, 146, DOI: **10.1007/s00604-025-07024-0**.

15 S. Sahoo, K. Y. Wickramathilaka, E. Njeri, D. Silva and S. L. Suib, A review on transition metal oxides in catalysis, *Front. Chem.*, 2024, **12**, 1–14, DOI: **10.3389/fchem.2024.1374878**.

16 A. S. Agnihotri, A. Varghese and M. Nidhin, Transition metal oxides in electrochemical and bio sensing: A state-of-art review, *Appl. Surf. Sci. Adv.*, 2021, **4**, 100072, DOI: **10.1016/j.apsadv.2021.100072**.

17 N. M. Hosny, I. Gomaa and M. G. Elmahgary, Adsorption of polluted dyes from water by transition metal oxides: A review, *Appl. Surf. Sci. Adv.*, 2023, **15**, 100395, DOI: **10.1016/j.apsadv.2023.100395**.

18 F. Ahmad, A. Shahzad, M. Danish, M. Fatima, M. Adnan and S. Atiq, *et al.*, Recent developments in transition metal oxide-based electrode composites for supercapacitor applications, *J. Energy Storage*, 2024, **81**, 110430, DOI: **10.1016/j.est.2024.110430**.

19 S. Steinhauer, Gas Sensors Based on Copper Oxide Nanomaterials: A Review, *Chemosensors*, 2021, **9**, 51, DOI: **10.3390/chemosensors9030051**.

20 S. Malik, J. Singh, R. Goyat, Y. Saharan, V. Chaudhry and A. Umar, *et al.*, Nanomaterials-based biosensor and their applications: A review, *Heliyon*, 2023, **9**, e19929, DOI: 10.1016/j.heliyon.2023.e19929.
21 N. Chakraborty, J. Banerjee, P. Chakraborty, A. Banerjee, S. Chanda and K. Ray, *et al.*, Green synthesis of copper/copper oxide nanoparticles and their applications: a review, *Green Chem. Lett. Rev.*, 2022, **15**, 187–215, DOI: 10.1080/17518253.2022.2025916.
22 M. H. Saleem, U. Ejaz, M. Vithanage, N. Bolan and K. H. M. Siddique, Synthesis, characterization, and advanced sustainable applications of copper oxide nanoparticles: a review, *Clean Technol. Environ. Policy*, 2024, DOI: 10.1007/s10098-024-02774-6.
23 T. Ringu, A. Das, S. Ghosh and N. Pramanik, Exploring the potential of copper oxide nanoparticles (CuO NPs) for sustainable environmental bioengineering applications, *Nanotechnol. Environ. Eng.*, 2024, **9**, 679–707, DOI: 10.1007/s41204-024-00389-2.
24 C. O. Aniagor, C. A. Igwegbe, K. O. Iwuozor, F. U. Iwuchukwu, S. Eshiemogie and M. C. Menkiti, *et al.*, CuO nanoparticles as modifiers for membranes: A review of performance for water treatment, *Mater. Today Commun.*, 2022, **32**, 103896, DOI: 10.1016/j.mtcomm.2022.103896.
25 M. Madani, S. Hosny, D. M. Alshangiti, N. Nady, S. A. Alkhursani and H. Alkhaldi, *et al.*, Green synthesis of nanoparticles for varied applications: Green renewable resources and energy-efficient synthetic routes, *Nanotechnol. Rev.*, 2022, **11**, 731–759, DOI: 10.1515/ntrev-2022-0034.
26 S. Kundu, V. Maheshwari, S. Niu and R. F. Saraf, Polyelectrolyte mediated scalable synthesis of highly stable silver nanocubes in less than a minute using microwave irradiation, *Nanotechnology*, 2008, 19, DOI: 10.1088/0957-4484/19/6/065604.
27 K. Okitsu, Y. Mizukoshi, T. A. Yamamoto, Y. Maeda and Y. Nagata, Sonochemical synthesis of gold nanoparticles on chitosan, *Mater. Lett.*, 2007, **61**, 3429–3431, DOI: 10.1016/j.matlet.2006.11.090.
28 D. Kirubakaran, J. B. A. Wahid and N. Karmegam, *et al.*, A Comprehensive Review on the Green Synthesis of Nanoparticles: Advancements in Biomedical and Environmental Applications, *Biomed. Mater. & Devices*, 2026, **4**, 388–413, DOI: 10.1007/s44174-025-00295-4.
29 R. S. Varma, Greener approach to nanomaterials and their sustainable applications, *Curr. Opin. Chem. Eng.*, 2012, **1**, 123–128, DOI: 10.1016/j.coche.2011.12.002.
30 M. F. Lengke, M. E. Fleet and G. Southam, Biosynthesis of silver nanoparticles by filamentous cyanobacteria from a silver(I) nitrate complex, *Langmuir*, 2007, **23**, 2694–2699, DOI: 10.1021/la0613124.
31 K. Govindaraju, S. K. Basha, V. G. Kumar and G. Singaravelu, Silver, gold and bimetallic nanoparticles production using single-cell protein (Spirulina platensis) Geitler, *J. Mater. Sci.*, 2008, **43**, 5115–5122, DOI: 10.1007/s10853-008-2745-4.
32 D. Rautaray, A. Ahmad and M. Sastry, Biosynthesis of CACO3 Crystals of Complex Morphology Using a Fungus and an Actinomycete, *J. Am. Chem. Soc.*, 2003, **125**, 14656–14657, DOI: 10.1021/ja0374877.
33 S. Jadoun, R. Arif, N. K. Jangid and R. K. Meena, Green synthesis of nanoparticles using plant extracts: a review, *Environ. Chem. Lett.*, 2021, **19**, 355–374, DOI: 10.1007/s10311-020-01074-x.
34 A. Gour and N. K. Jain, Advances in green synthesis of nanoparticles, *Artif. Cells, Nanomed., Biotechnol.*, 2019, **47**, 844–851, DOI: 10.1080/21691401.2019.1577878.
35 E. Hosseinzadeh, A. Foroumadi and L. Firoozpour, What is the role of phytochemical compounds as capping agents for the inhibition of aggregation in the green synthesis of metal oxide nanoparticles? A DFT molecular level response, *Inorg. Chem. Commun.*, 2023, **147**, 110243, DOI: 10.1016/j.inoche.2022.110243.
36 P. B. Chouke, T. Shrirame, A. K. Potbhare, A. Mondal, A. R. Chaudhary and S. Mondal, *et al.*, Bioinspired metal/metal oxide nanoparticles: A road map to potential applications, *Mater. Today Adv.*, 2022, **16**, 100314, DOI: 10.1016/j.mtadv.2022.100314.
37 S. K. Bhagat, K. E. Pilario, O. E. Babalola, T. Tiyasha, M. Yaqub and C. E. Onu, *et al.*, Comprehensive review on machine learning methodologies for modeling dye removal processes in wastewater, *J. Cleaner Prod.*, 2023, **385**, 135522, DOI: 10.1016/j.jclepro.2022.135522.
38 I. Dahlan, O. H. Keat, H. A. Aziz and Y.-T. Hung, Synthesis and characterization of MOF-5 incorporated waste-derived siliceous materials for the removal of malachite green dye from aqueous solution, *Sustainable Chem. Pharm.*, 2023, **31**, 100954, DOI: 10.1016/j.scp.2022.100954.
39 K. S. Obayomi, S. Y. Lau, O. Ibrahim, J. Zhang, L. Meunier and M. M. Aniobi, *et al.*, Removal of Congo red dye from aqueous environment by zinc terephthalate metal organic framework decorated on silver nanoparticles-loaded biochar: Mechanistic insights of adsorption, *Microporous Mesoporous Mater.*, 2023, **355**, 112568, DOI: 10.1016/j.micromeso.2023.112568.
40 S. Dan, H. Bagheri, A. Shahidizadeh and H. Hashemipour, Performance of graphene Oxide/SiO_2 Nanocomposite-based: Antibacterial Activity, dye and heavy metal removal, *Arab. J. Chem.*, 2023, **16**, 104450, DOI: 10.1016/j.arabjc.2022.104450.
41 M. Ahmadian and M. Jaymand, Interpenetrating polymer network hydrogels for removal of synthetic dyes: A comprehensive review, *Coord. Chem. Rev.*, 2023, **486**, 215152, DOI: 10.1016/j.ccr.2023.215152.
42 Y. Liu, A.-A. Yang, X.-S. Zhang, Z.-B. Sun, W.-Z. Li and Y. Wang, *et al.*, Synthesis of metal–organic coordination polymers and their derived nanostructures for organic dye removal and analyte detection, *J. Environ. Chem. Eng.*, 2022, **10**, 108215, DOI: 10.1016/j.jece.2022.108215.
43 T. S. Vo, M. M. Hossain, T. Lim, J. W. Suk, S. Choi and K. Kim, Modification of the interfacial glass fiber surface through graphene oxide-chitosan interactions for excellent dye removal as an adsorptive membrane, *J. Environ. Chem. Eng.*, 2022, **10**, 108965, DOI: 10.1016/j.jece.2022.108965.

44 N. Vasiraja, R. Saravana Sathiya Prabhahar and A. Joshua, Preparation and Physio–Chemical characterisation of activated carbon derived from prosopis juliflora stem for the removal of methylene blue dye and heavy metal containing textile industry effluent, *J. Cleaner Prod.*, 2023, **397**, 136579, DOI: **10.1016/j.jclepro.2023.136579**.

45 S. S. Mohammed Ameen, D. D. Hassan, D. S. Mohammed, K. M. Omer, D. A. Latif and Y. O. Mohammad, Natural-based chalcopyrite nanoparticles as high-performance mineral adsorbents for organic dye removal in water, *Mater. Adv.*, 2025, **6**, 2192–2201, DOI: **10.1039/D5MA00038F**.

46 J. Hu, Y. Xu, X. Zheng, Y. Pan, J. Wang and T. Shu, *et al.*, Construction Iron-based metal organic frameworks based on ligand engineering for selective dyes removal from water solution, *Inorg. Chem. Commun.*, 2023, **147**, 110183, DOI: **10.1016/j.inoche.2022.110183**.

47 K. M. A. Qasem, S. Khan, S. Chinnam, H. A. M. Saleh, I. Mantasha and M. Zeeshan, *et al.*, Sustainable fabrication of Co-MOF@CNT nano-composite for efficient adsorption and removal of organic dyes and selective sensing of Cr(VI) in aqueous phase, *Mater. Chem. Phys.*, 2022, **291**, 126748, DOI: **10.1016/j.matchemphys.2022.126748**.

48 S. I. Siddiqui, E. S. Allehyani, S. A. Al-Harbi, Z. Hasan, M. A. Abomuti and H. K. Rajor, *et al.*, Investigation of Congo Red Toxicity towards Different Living Organisms: A Review, *Processes*, 2023, **11**, 807, DOI: **10.3390/pr11030807**.

49 P. O. Oladoye, M. O. Bamigboye, O. D. Ogunbiyi and M. T. Akano, Toxicity and decontamination strategies of Congo red dye, *Groundw. Sustainable Dev.*, 2022, **19**, 100844, DOI: **10.1016/j.gsd.2022.100844**.

50 G. E.-S. Batiha, S. T. Tene, J. O. Teibo, H. M. Shaheen, O. S. Oluwatoba and T. K. A. Teibo, *et al.*, The phytochemical profiling, pharmacological activities, and safety of *malva sylvestris*: a review, *Naunyn Schmiedebergs Arch. Pharmacol.*, 2023, **396**, 421–440, DOI: **10.1007/s00210-022-02329-w**.

51 A. F. Al-Rubaye, A. F. Kaizal and I. H. Hameed, Phytochemical Screening of Methanolic Leaves Extract of *Malva sylvestris*, *Int. J. Pharmacogn. Phytochem. Res.*, 2017, **9**, 537–552, DOI: **10.25258/phyto.v9i4.8127**.

52 A. Deb, A. Debnath, N. Bhattacharjee and B. Saha, Ultrasonically enhanced dye removal using conducting polymer functionalised ZnO nanocomposite at near neutral pH: kinetic study, isotherm modelling and adsorbent cost analysis, *Int. J. Environ. Anal. Chem.*, 2022, **102**, 8055–8074, DOI: **10.1080/03067319.2020.1843649**.

53 A. Deb, A. Debnath and B. Saha, Ultrasound-aided rapid and enhanced adsorption of anionic dyes from binary dye matrix onto novel hematite/polyaniline nanocomposite: Response surface methodology optimization, *Appl. Organomet. Chem.*, 2020, **34**, e5353, DOI: **10.1002/aoc.5353**.

54 M. Chen, X. He, H. Sun, Y. Sun, L. Li and J. Zhu, Phytochemical analysis, UPLC-ESI-Orbitrap-MS analysis, biological activity, and toxicity of extracts from Tripleurospermum limosum (Maxim.), *Pobed. Arab J. Chem.*, 2022, **15**, 1–29, DOI: **10.1016/j.arabjc.2022.103797**.

55 V. Singh and R. Kumar, Study of Phytochemical Analysis and Antioxidant Activity of Allium sativum of Bundelkhand Region, *Int. J. Life Sci. Res.*, 2017, **3**, 1451–1458, DOI: **10.21276/ijlssr.2017.3.6.4**.

56 S. Singh, R. Nigam, A. Sharma, A. Kumar and V. Laxmi, Preliminary Phytochemical Screening of Elytraria acaulis Roots, *J. Pharm. Res. Int.*, 2021, **33**, 1–9, DOI: **10.9734/JPRI/2021/v33i431165**.

57 S. Nirmalraj and K. Perinbam, Studies on Phytochemical Screening and in vitro Antioxidant Activity of Ethyl Acetate Leaf Extract of Justicia gendarussa Burm. F, *Res. J. Bot.*, 2015, **10**, 30–36, DOI: **10.3923/rjb.2015.30.36**.

58 G. A. Omar and L. Y. Mohammed, Physiochemical standardization and phytochemical screening of Urtica dioica L. Leaves Growing In Zakho, Kurdistan Region, Iraq, *Sci. J. Univ. Zakho*, 2023, **11**, 306–316, DOI: **10.25271/sjuoz.2023.11.3.1069**.

59 S. S. Mohsen Ali and P. Robin, Comprehensive phytochemical profiling of bioactive compounds from Barleria prattensis for their antioxidant and cytotoxic capacity and its characterization using GC-MS, *Biochem. Biophys. Rep.*, 2025, **43**, 102083, DOI: **10.1016/j.bbrep.2025.102083**.

60 N. Porwal, D. B. Gupta, A. K. Gakkhar, R. C. Tiwari and B. Mittal, An Evaluation of Physicochemical Parameters and Quantitative Phytochemical Analysis of Datura Metel-A Research Article, *J. Ayurvedic Herb. Integr. Med.*, 2023, **3**, 1–13, DOI: **10.29121/jahim.v3.i2.2023.30**.

61 M. Mohlakoana and A. Moteetee, Southern African Soap Plants and Screening of Selected Phytochemicals and Quantitative Analysis of Saponin Content, *Resources*, 2021, **10**, 96, DOI: **10.3390/resources10100096**.

62 A. Benhammada and D. Trache, Green synthesis of CuO nanoparticles using *Malva sylvestris* leaf extract with different copper precursors and their effect on nitrocellulose thermal behavior, *J. Therm. Anal. Calorim.*, 2022, **147**, 1–16, DOI: **10.1007/s10973-020-10469-5**.

63 R. Lafi, I. Montasser and A. Hafiane, Adsorption of congo red dye from aqueous solutions by prepared activated carbon with oxygen-containing functional groups and its regeneration, *Adsorpt. Sci. Technol.*, 2019, **37**, 160–181, DOI: **10.1177/0263617418819227**.

64 G. M. A. Mahran, M. A. Gado, W. M. Fathy and A. B. ElDeeb, Eco-Friendly Recycling of Lithium Batteries for Extraction of High-Purity Metals, *Materials*, 2023, **16**, 4662, DOI: **10.3390/ma16134662**.

65 M. Mohery, G. M. A. Mahran, B. M. Atia and M. A. Gado, Removal of lead ions from wastewater by a new chelating amidoxime based-mesoporous silica, *Inorg. Chem. Commun.*, 2025, **180**, 114884, DOI: **10.1016/j.inoche.2025.114884**.

66 I. Aminu, S. M. Gumel, W. A. Ahmad and A. A. Idris, Adsorption Isotherms and Kinetic Studies of Congo-Red Removal from Waste Water Using Activated Carbon Prepared from Jujube Seed, *Am. J. Anal. Chem.*, 2020, **11**, 47–59, DOI: **10.4236/ajac.2020.111004**.

67 A. Pratt, *Environmental applications of magnetic nanoparticles*, Elsevier Ltd., 1st edn, vol. 6, 2014, DOI: 10.1016/B978-0-08-098353-0.00007-5.

68 A. M. Amin, H. A. Ibrahium, A. A. Gouda, R. E. Sheikh, B. M. Atia and M. A. Gado, *et al.*, Design and utilisation of a novel poly imino-phosphorane composite for the effective removal of Pb 2+ and Cr 3+ ions from contaminated water sources, *Int. J. Environ. Anal. Chem.*, 2024, 1–28, DOI: 10.1080/03067319.2024.2420827.

69 S. A. Mahmoud, B. M. Atia and M. A. Gado, Efficient removal of toxic metals (Hg(II), Cr(III), Pb(II), Cd(II)) using high-performance polyvinyl alcohol-L-2-Amino-3-mercaptopropionic acid composite from wastewater, *Int. J. Environ. Sci. Technol.*, 2025, **22**, 12269–12294, DOI: 10.1007/s13762-025-06395-4.

70 P. Das, S. Nisa, A. Debnath and B. Saha, Enhanced adsorptive removal of toxic anionic dye by novel magnetic polymeric nanocomposite: optimization of process parameters, *J. Dispers. Sci. Technol.*, 2022, **43**, 880–895, DOI: 10.1080/01932691.2020.1845958.

71 S. A. Mahmoud, L. Galal Amin, B. M. Atia and M. Gado, Sustainable recovery of silver from X-ray film processing effluents using a novel thiourea derivative-grafted XAD-7 resin and its application in nano silver particle synthesis, *Int. J. Environ. Anal. Chem.*, 2025, 1–33, DOI: 10.1080/03067319.2025.2505934.

72 N. Benhadria, M. Hachemaoui, F. Zaoui, A. Mokhtar, S. Boukreris and T. Attar, *et al.*, Catalytic Reduction of Methylene Blue Dye by Copper Oxide Nanoparticles, *J. Clust. Sci.*, 2022, **33**, 249–260, DOI: 10.1007/s10876-020-01950-0.

73 M. Ghulam, T. Hajira, S. Muhammad and A. Nasir, Synthesis and characterization of cupric oxide (CuO) nanoparticles and their application for the removal of dyes, *African J. Biotechnol.*, 2013, **12**, 6650–6660, DOI: 10.5897/AJB2013.13058.

74 A. Bavi, M. S. Jafari, M. Heydari, F. Ebrahimi and A. Sadeghizadeh, Batch and continuous mode adsorption of methylene blue cationic dye onto synthesized titanium dioxide/polyurethane nanocomposite modified by sodium dodecyl sulfate, *Colloids Surf., C*, 2023, **1**, 100012, DOI: 10.1016/j.colsuc.2023.100012.

75 M. B. Mobarak, M. F. Sikder, K. S. Muntaha, S. Islam, S. M. F. Rabbi and F. Chowdhury, Plant extract-mediated green-synthesized CuO nanoparticles for environmental and microbial remediation: a review covering basic understandings to mechanistic study, *Nanoscale Adv.*, 2025, **7**, 2418–2445, DOI: 10.1039/d5na00035a.

76 D. Letchumanan, S. P. M. Sok, S. Ibrahim, N. H. Nagoor and N. M. Arshad, Plant-Based Biosynthesis of Copper/Copper Oxide Nanoparticles: An Update on Their Applications in Biomedicine, Mechanisms, and Toxicity, *Biomolecules*, 2021, **11**, 564, DOI: 10.3390/biom11040564.

77 W. Zhang, In Nanoparticle Aggregation: Principles and Modeling, ed D. G. Capco, Y. Chen, *Nanomaterial*, Springer Netherlands, Dordrecht, 2014, pp. 19–43, DOI: 10.1007/978-94-017-8739-0_2.

78 J. Kumar, M. S. Akhtar, S. Ameen, P. Srivastava and G. Singh, Green synthesis of CuO nanoparticles with leaf extract of Calotropis gigantea and its dye-sensitized solar cells applications, *J. Alloys Compd.*, 2015, **632**, 321–325, DOI: 10.1016/j.jallcom.2015.01.172.

79 K. Velsankar, S. Suganya, P. Muthumari, S. Mohandoss and S. Sudhahar, Journal of Environmental Chemical Engineering Ecofriendly green synthesis, characterization and biomedical applications of CuO nanoparticles synthesized using leaf extract of Capsicum frutescens, *J. Environ. Chem. Eng.*, 2021, **9**, 106299, DOI: 10.1016/j.jece.2021.106299.

80 S. Dubey and Y. C. Sharma, Calotropis procera mediated one pot green synthesis of Cupric oxide nanoparticles (CuO-NPs) for adsorptive removal of Cr(VI) from aqueous solutions, *Appl. Organomet. Chem.*, 2017, **31**, 1–15, DOI: 10.1002/aoc.3849.

81 S. Surendhiran, V. Gowthambabu, A. Balamurugan, M. Sudha, V. B. Senthil Kumar and K. C. Suresh, Rapid green synthesis of CuO nanoparticles and evaluation of its photocatalytic and electrochemical corrosion inhibition performance, *Mater. Today Proc.*, 2021, **47**, 1011–1016, DOI: 10.1016/j.matpr.2021.05.515.

82 E. Yousef, M. Salah, H. A. Yousef, M. Ibrahim, M. S. Mostafa and H. M. A. Elkabeer, *et al.*, Electrospun nanofibrous scaffolds of polylactic acid loaded with ginger/MoO3/CuO/graphene oxide: biocompatibility and antibacterial activity, *Polym. Bull.*, 2024, **81**, 12921–12946, DOI: 10.1007/s00289-024-05322-w.

83 A. Mulik, P. Hegade, S. Mulik and M. Deshmukh, CuO nanoparticles and nanobelts catalyzed potent synthesis of benzopyran derivatives, *Res. Chem. Intermed.*, 2019, **45**, 5641–5647, DOI: 10.1007/s11164-019-03925-x.

84 K. Kannan, D. Radhika, S. Vijayalakshmi, K. K. Sadasivuni, A. A. Ojiaku and U. Verma, Facile fabrication of CuO nanoparticles *via* microwave-assisted method: photocatalytic, antimicrobial and anticancer enhancing performance, *Int. J. Environ. Anal. Chem.*, 2022, **102**, 1095–1108, DOI: 10.1080/03067319.2020.1733543.

85 Z. Alhalili, Green synthesis of copper oxide nanoparticles CuO NPs from Eucalyptus Globoulus leaf extract: Adsorption and design of experiments, *Arab. J. Chem.*, 2022, **15**, 103739, DOI: 10.1016/j.arabjc.2022.103739.

86 J. Neiva, Z. Benzarti, S. Carvalho and S. Devesa, Green Synthesis of CuO Nanoparticles—Structural, Morphological, and Dielectric Characterization, *Materials*, 2024, **17**, 5709, DOI: 10.3390/ma17235709.

87 M. E. H. Naghi Tehrani, P. Ghahremani, M. Ramezanzadeh, G. Bahlakeh and B. Ramezanzadeh, Theoretical and experimental assessment of a green corrosion inhibitor extracted from *Malva sylvestris*, *J. Environ. Chem. Eng.*, 2021, **9**, 105256, DOI: 10.1016/j.jece.2021.105256.

88 V. Uddin, A. Ansari, R. Chauhan and W. Ahmad, Green synthesis of copper oxide (CuO) nanoparticles by Punica granatum peel extract Materials Today: Proceedings Green synthesis of copper oxide (CuO) nanoparticles by Punica granatum peel extract, *Mater. Today Proc.*, 2020, **36**, 751–755, DOI: 10.1016/j.matpr.2020.05.504.

89 F. Amin, Fozia, B. Khattak, A. Alotaibi, M. Qasim and I. Ahmad, *et al.*, Green Synthesis of Copper Oxide Nanoparticles Using Aerva javanica Leaf Extract and Their Characterization and Investigation of In Vitro Antimicrobial Potential and Cytotoxic Activities, *J. Evidence-Based Complementary Altern. Med.*, 2021, **2021**, 1–12, DOI: 10.1155/2021/5589703.

90 C. Rey, V. Renugopalakrishman, B. Collins and M. J. Glimcher, Fourier transform infrared spectroscopic study of the carbonate ions in bone mineral during aging, *Calcif. Tissue Int.*, 1991, **49**, 251–258, DOI: 10.1007/BF02556214.

91 A. Matei, G. Craciun, C. Romanitan, C. Pachiu and V. Tucureanu, Biosynthesis and Characterization of Copper Oxide Nanoparticles, *Eng. Proc.*, 2023, 37, DOI: 10.3390/ECP2023-14629.

92 H. Abdollahzadeh, Y. Pazhang, A. Zamani and Y. Sharafi, Green synthesis of copper oxide nanoparticles using walnut shell and their size dependent anticancer effects on breast and colorectal cancer cell lines, *Sci. Rep.*, 2024, **14**, 1–18, DOI: 10.1038/s41598-024-71234-4.

93 K. Ssekatawa, D. K. Byarugaba, M. K. Angwe, E. M. Wampande, F. Ejobi and E. Nxumalo, *et al.*, Phyto-Mediated Copper Oxide Nanoparticles for Antibacterial, Antioxidant and Photocatalytic Performances, *Front. Bioeng. Biotechnol.*, 2022, **10**, 1–17, DOI: 10.3389/fbioe.2022.820218.

94 K. Kaur, S. Yamini, J. V. Reshma, G. Lakshmi, K. Parikshit, R. K. C. Vagdevi and S. Subhadip, *et al.*, Green synthesis of saponin-capped copper (II) oxide (CuO) nanoparticles and their efficacy in photocatalytic dye degradation, *Sustainable Chem. One World*, 2025, **6**, 100054, DOI: 10.1016/j.scowo.2025.100054.

95 R. Gaurav Sharma, Pterocarpus marsupium Derived Phyto-Synthesis of Copper Oxide Nanoparticles and their Antimicrobial Activities, *J. Microb. Biochem. Technol.*, 2015, **07**, 3–8, DOI: 10.4172/1948-5948.1000195.

96 A. M. Eid, A. Fouda, S. E. D. Hassan, M. F. Hamza, N. K. Alharbi and A. Elkelish, *et al.*, Plant-Based Copper Oxide Nanoparticles; Biosynthesis, Characterization, Antibacterial Activity, Tanning Wastewater Treatment, and Heavy Metals Sorption, *Catalysts*, 2023, 13, DOI: 10.3390/catal13020348.

97 N. Baylan, İ. İlalan and İ. İnci, Copper Oxide Nanoparticles as a Novel Adsorbent for Separation of Acrylic Acid from Aqueous Solution: Synthesis, Characterization, and Application, *Water, Air, Soil Pollut.*, 2020, **231**, 465, DOI: 10.1007/s11270-020-04832-3.

98 L. Dörner, C. Cancellieri, B. Rheingans, M. Walter, R. Kägi and P. Schmutz, *et al.*, Cost-effective sol-gel synthesis of porous CuO nanoparticle aggregates with tunable specific surface area, *Sci. Rep.*, 2019, **9**, 11758, DOI: 10.1038/s41598-019-48020-8.

99 K. Shola, S. Yon, M. K. Danquah, J. Zhang, T. Chiong and O. Victoria, *et al.*, A response surface methodology approach for the removal of methylene blue dye from wastewater using sustainable and cost-effective adsorbent, *Process Saf. Environ. Prot.*, 2024, **184**, 129–150, DOI: 10.1016/j.psep.2024.01.106.

100 P. Palai, S. Muduli, B. Priyadarshini and T. R. Sahoo, A facile green synthesis of ZnO nanoparticles and its adsorptive removal of Congo red dye from aqueous solution, *Mater. Today Proc.*, 2020, **38**, 2445–2451, DOI: 10.1016/j.matpr.2020.07.387.

101 I. Ali, Z. A. Al-othman and A. Alwarthan, Molecular uptake of congo red dye from water on iron composite nano particles, *J. Mol. Liq.*, 2016, **224**, 171–176, DOI: 10.1016/j.molliq.2016.09.108.

102 V. S. Sousa and M. R. Teixeira, Aggregation kinetics and surface charge of CuO nanoparticles: the influence of pH, ionic strength and humic acids, *Environ. Chem.*, 2013, **10**, 313, DOI: 10.1071/EN13001.

103 R. Khan, M. A. Inam, D. R. Park, S. Khan, M. Akram and I. T. Yeom, The Removal of CuO Nanoparticles from Water by Conventional Treatment C/F/S: The Effect of pH and Natural Organic Matter, *Molecules*, 2019, **24**, 914, DOI: 10.3390/molecules24050914.

104 A. Radwan, S. O. Mohamed, M. M. H. Khalil and I. M. El-Sewify, Effective adsorption of fluorescent congo red azo dye from aqueous solution by green synthesized nanosphere ZnO/CuO composite using propolis as bee byproduct extract, *Sci. Rep.*, 2024, **14**, 1–12, DOI: 10.1038/s41598-024-58306-1.

105 F. J. Alguacil and F. A. López, Organic Dyes *versus* Adsorption Processing, *Molecules*, 2021, **26**, 5440, DOI: 10.3390/molecules26185440.

106 A. A. Haji, R. S. Abduljabar, S. A. Yasin, Z. A. Omar, H. A. Ahmed and M. A. Assiri, *et al.*, Green Synthesis of Magnetite Nanoparticles Mediated Fumaria officinalis L. Plant as Sustainable and Renewable Adsorbing Materials, *Separations*, 2023, **10**, 518, DOI: 10.3390/separations10090518.

107 S. Kalam, S. A. Abu-Khamsin, M. S. Kamal and S. Patil, Surfactant Adsorption Isotherms: A Review, *ACS Omega*, 2021, **6**, 32342–32348, DOI: 10.1021/acsomega.1c04661.

108 A. A. Haji, N. Meena, S. Mohammed, P. Peel and H. Metal, Optimization of arsenic adsorption onto activated carbon of, *Sci. J. Univ. Zakho*, 2019, **7**, 37–44, DOI: 10.25271/sjuoz.2019.7.2.594.

109 P. Das, A. Debnath and B. Saha, Ultrasound-assisted enhanced and rapid uptake of anionic dyes from the binary system onto MnFe2O4/polyaniline nanocomposite at neutral pH, *Appl. Organomet. Chem.*, 2020, **34**, 1–16, DOI: 10.1002/aoc.5711.

110 Saruchi and V. Kumar, Adsorption kinetics and isotherms for the removal of rhodamine B dye and Pb +2 ions from aqueous solutions by a hybrid ion-exchanger, *Arab. J. Chem.*, 2019, **12**, 316–329, DOI: 10.1016/j.arabjc.2016.11.009.

111 M. Zeeshan, T. Javed, C. Kumari, A. Thumma, M. Wasim and M. B. Taj, *et al.*, Investigating the interactions between dyes and porous/composite materials: A comprehensive study, *Sustainable Chem. Environ.*, 2025, **9**, 100217, DOI: 10.1016/j.scenv.2025.100217.

112 A. Deb, A. Debnath and B. Saha, Sono-assisted enhanced adsorption of eriochrome Black-T dye onto a novel polymeric nanocomposite: kinetic, isotherm, and response surface methodology optimization, *J. Dispers. Sci. Technol.*, 2021, **42**, 1579–1592, DOI: 10.1080/01932691.2020.1775093.

113 W. Jadaa, Wastewater Treatment Utilizing Industrial Waste Fly Ash as a Low-Cost Adsorbent for Heavy Metal Removal: Literature Review, *Clean Technol.*, 2024, **6**, 221–279, DOI: **10.3390/cleantechnol6010013**.

114 B. A. Ejeta, G. F. Aaga, W. M. Fereja and B. Mengesha, Biofabrication of highly effective and easily regenerated CuO nanoparticles as adsorbents for Congo red and malachite green removal, *Sci. Rep.*, 2024, **14**, 24116, DOI: **10.1038/s41598-024-74974-5**.

115 M. Taha, M. Abbas, E. M. Ali, H. Fakhry and A. Elsayed, Bioremediation of Congo red Dyes using Biosynthesized copper/iron Nanoparticles, *Egypt J. Chem.*, 2024, **67**, 527–541, DOI: **10.21608/EJCHEM.2023.213599.8030**.

116 H. Abbas, M. Tahir, W. Qayyum, S. Tariq, T. Munawar and M. Ismaeel, *et al.*, Synthesis of Mg-Doped CuO Nanoparticles for Efficient Removal of Congo Red Dye from Wastewater: Adsorption Study, *Asian J. Chem. Sci.*, 2023, **13**, 94–105, DOI: **10.9734/ajocs/2023/v13i6265**.